THE JOURNAL OF PHYSICAL CHEMISTRY C

Article

Cite This: J. Phys. Chem. C 2019, 123, 24453−24460

pubs.acs.org/JPCC

Understanding the Impact of *N*-Arylpyridinium Ions on the Selectivity of CO_2 Reduction at the Cu/Electrolyte Interface

Vincent J. Ovalle and Matthias M. Waegele*

Department of Chemistry, Merkert Chemistry Center, Boston College, Chestnut Hill, Massachusetts 02467, United States

Supporting Information

ABSTRACT: Copper is the only pure metal electrocatalyst capable of converting carbon dioxide to hydrocarbons at significant reaction rates. However, the poor product selectivity of this process on copper remains a critical challenge. Modification of the aqueous electrolyte/copper interface with organic thin films has emerged as a promising means for tuning the selectivity toward valuable $C_{\geq 2}$ hydrocarbons. Recently, it was demonstrated that the addition of *N*-substituted arylpyridinium derivatives to the electrolyte substantially alters the reaction selectivity (Han et al. *ACS Cent. Sci.* **2017**, *3*, 853−859). The changes in selectivity were shown to sensitively depend on the chemical structure of the added *N*-substituted arylpyridinium. For example, 1-(4-tolyl)pyridinium (T-Pyr) increases the Faradaic efficiency of $C_{\geq 2}$ products to ≈80% (compared to ≈25% observed for the unmodified Cu/electrolyte interface), whereas 1-(4-pyridyl)pyridinium (P-Pyr) blocks the pathways to $C_{\geq 2}$ products. It has been demonstrated that the reduction of *N*-substituted arylpyridinium derivatives leads to the formation of organic thin films on Cu electrodes. However, the mechanisms by which these thin films regulate the reaction selectivity are poorly understood. Herein, using surface-enhanced infrared absorption spectroscopy, we elucidate how films formed from T-Pyr and P-Pyr give rise to distinct interfacial properties that result in the observed differences in catalytic selectivity. We find that the two films alter the reactivity of the surface in two distinct ways: (1) in the presence of T-Pyr, the interfacial pH increases at moderate current densities (<5 mA cm^{-2}), as evidenced by the appearance of a carbonate absorption band in the infrared spectrum of the interface. By contrast, the band of solution carbonate is comparatively small or absent in the spectra of the unmodified Cu/electrolyte contact and the corresponding interface modified by P-Pyr. Scanning electron microscopy of the modified Cu surfaces reveals that the T-Pyr- and P-Pyr-derived films exhibit distinct morphologies. Taken together, these observations suggest that the film formed by T-Pyr leads to an increase in the interfacial pH by limiting the mass transport to/from the interface. Therefore, the favorable selectivity for $C_{\geq 2}$ products is a result of the limited proton availability at that interface. (2) In the presence of P-Pyr, the lineshape of the C≡O stretch band of atop-bound CO (CO_{atop}) is markedly different from that of CO_{atop} on unmodified and T-Pyr-modified Cu electrodes. Using pyridine, we show that N-heterocycles with a lone pair on the nitrogen atom (such as P-Pyr) compete with CO for undercoordinated Cu sites. On the basis of these results, we conclude that the selective poisoning of these undercoordinated Cu sites impedes the reduction of the CO intermediate to higher order reduction products in the presence of P-Pyr. Taken together, our results explain the observed reactivity trends in terms of the altered interfacial properties in the presence of the films. Our study further implicates undercoordinated Cu sites as catalytically active sites in the reduction of CO to hydrocarbons.

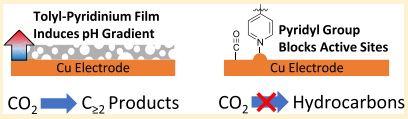

Downloaded via BOSTON COLG on May 1, 2020 at 00:12:06 (UTC).
See https://pubs.acs.org/sharingguidelines for options on how to legitimately share published articles.

INTRODUCTION

Among all pure metal electrodes, Cu exhibits the largest Faradaic current densities for the aqueous electrochemical reduction of carbon dioxide to hydrocarbons (≈5 mA cm^{-2}).[1,2] However, the reaction selectivity of the process on this catalyst is poor.[3−6] Multiple products, such as methane, ethylene, formate, and CO, form simultaneously during electrolysis. A significant portion of the Faradaic current arises from the competing reduction of protons to hydrogen gas. Increasing the product selectivity toward valuable hydrocarbon products, such as ethylene or ethanol, is essential for making this process economically viable.[7−9] The product distribution is greatly impacted by the reaction conditions and the surface structure of the Cu electrode. For example, electrolytes with basic pH[3,10,11] and electrodes with high densities of under-coordinated Cu atoms[12−17] have been shown to favor the formation of valuable hydrocarbons and oxygenates. On the basis of these findings, the judicious choice of process conditions and electrode morphology has enabled the conversion of CO_2 and CO to $C_{\geq 2}$ hydrocarbons with selectivities of >70%.[14,18−21] Despite this recent success, further improvements in catalytic selectivity and stability are necessary.

A complementary approach to tuning the pH of the electrolyte and the electrode's surface structure is the modification of the electrode surface with organic additives.[22−35] For example, during the reduction of CO_2 on Ag electrodes, diaminotriazole improves the selectivity toward CO relative to the formation of hydrogen by 1 order of magnitude compared to the selectivity in the absence of this additive.[23,36] On p-type GaP, the photo-driven reduction of CO_2 to

Received: September 11, 2019
Published: September 17, 2019

© 2019 American Chemical Society

DOI: 10.1021/acs.jpcc.9b08666
J. Phys. Chem. C 2019, 123, 24453−24460

methanol proceeds with a Faradaic efficiency close to 100% in the presence of pyridinium.[22] Decoration of Au and Cu electrodes with certain organic compounds is also a promising strategy: in comparison to the respective unmodified electrodes, enhancements of the selectivities toward desirable products on the order of a factor of 2 have been reported for Au and Cu electrodes functionalized with amino acids,[24] thiol-containing compounds,[25] and polyamides.[29] Han et al. have reported selectivities of 70−80% for $C_{\geq 2}$ products on Cu electrodes modified by organic films derived from *N*-arylpyridinium compounds.[26]

The origins of these changes in selectivity can be manifold and may include the blocking of catalytic sites, modulation of the adsorption energies of reactive species, or alteration of the reaction pathway. Knowledge of the mechanism by which these surface modifications impact the product selectivity is essential for effectively altering the catalytic properties of the metal/electrolyte contact. However, these mechanisms remain largely unexplored to date.

Herein, using surface-enhanced infrared absorption spectroscopy (SEIRAS), we probed Cu/electrolyte interfaces modified by organic films derived from *N*-arylpyridinium compounds. We chose to study these systems for the following reasons:

1 These films have a large impact on the selectivity of electrochemical CO_2 reduction. Faradaic efficiencies of up to ≈80% for $C_{\geq 2}$ hydrocarbons were reported for the Cu/electrolyte interfaces modified by some of these organic films.[26]
2 The changes in selectivity are strongly dependent on the structure of the employed *N*-arylpyridinium compound. Although some derivatives were shown to greatly enhance the selectivity for $C_{\geq 2}$ hydrocarbons, others essentially blocked their formation. Therefore, these systems are ideal models to understand the interplay between different interfacial components and how this interplay impacts the observed selectivity.

RESULTS AND DISCUSSION

Choice of Additives. For this study, we chose two arylpyridinium derivatives that were reported to modulate the product distribution of CO_2 reduction on polycrystalline copper electrodes in distinct ways:[26] 1-(4-tolyl)pyridinium (T-Pyr) and 1-(4-pyridyl)pyridinium (P-Pyr). The chemical structures of these compounds are shown in Figure 1. The presence of either one of these compounds (10 mM) in the electrolyte results in their reductive deposition on the Cu electrode. In the case of T-Pyr, the deposit was shown to consist of a T-Pyr dimer (Figure 1).[26] The visible, white organic films formed from T-Pyr and P-Pyr distinctly affect the product selectivity of CO_2 reduction. The partial currents for the main products, as measured by Han et al.,[26] are summarized in Table 1. T-Pyr-derived films reduce the rates

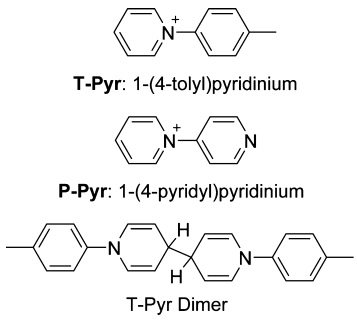

Figure 1. Chemical structures of T-Pyr, P-Pyr, and the T-Pyr dimer.

Table 1. Partial Current Densities of Various Reduction Products for Polycrystalline Cu Electrodes in the Presence and Absence of 10 mM T-Pyr/P-Pyr in CO_2-Saturated 0.1 M $KHCO_3$ at an Applied Potential of −1.1 V vs an RHE, as Reported by Han and Co-Workers[26]

	current density (mA cm^{-2})		
compound	CH_4	H_2	$C_{\geq 2}$
unmodified Cu	0.90	1.91	1.16
T-Pyr	0.01	0.16	0.80
P-Pyr	0.001	1.94	0.00

of methane and hydrogen formation by more than an order of magnitude compared to those observed on the unmodified Cu electrode, whereas the production rates for $C_{\geq 2}$ species (ethylene, ethanol, and propanol) are only slightly affected. By contrast, P-Pyr-derived films effectively shut down the formation of hydrocarbon species, whereas the rate of hydrogen evolution is not impeded. Herein, to identify the physical origins of these distinct impacts on the product distribution, we probed the Cu/electrolyte interfaces modified by T-Pyr and P-Pyr films with SEIRAS.

Formation of T-Pyr- and P-Pyr-Derived Films. We monitored the formation of the films in situ on Cu electrodes by cyclic voltammetry and SEIRAS. The electrodes were polycrystalline Cu thin films, electrolessly deposited onto a Si attenuated total reflection (ATR) element as described previously.[37] The electrolytes were CO_2-saturated aqueous solutions of 0.5 M $KHCO_3$ (pH 7.4) with and without 10 mM P-Pyr and T-Pyr. We employed a two-compartment spectroelectrochemical cell that permits stirring of the electrolyte (Figure S1 of the Supporting Information).[38] We collected the electrochemical currents and IR spectra of the Cu/electrolyte interface concurrently. Using this electrochemical setup and electrolyte, we observed film-induced changes in the product selectivity similar to those reported in Table 1 (Supporting Information, Table S1). Unless otherwise noted, all potentials reported herein are referenced against the silver/silver chloride electrode (Ag/AgCl).

Figure 2 shows the cyclic voltammograms with and without 10 mM P-Pyr and T-Pyr. In the absence of P-Pyr or T-Pyr, the reduction current density steeply and monotonically rises with a decreasing potential. By contrast, in the presence of either P-Pyr or T-Pyr, a reduction wave at ≈−0.9 V is observed. This wave is observed because of the reduction of P-Pyr and T-Pyr.[26] The reduction of either of these species results in the formation of a white film on the Cu electrode. In the case of T-Pyr, ex situ nuclear magnetic resonance (NMR) spectroscopy has shown that the reduced species is a hydrogenated T-Pyr dimer.[26] Figure 3A shows the spectra of the Cu/electrolyte interfaces at a potential of −1.1 V, where the films have formed. The reported spectra are based on a reference spectrum taken before the addition of T-Pyr and P-Pyr to the electrolyte. Therefore, the spectra contain features of the solid film and solution species. The potential dependence of the spectra and the various bands is further discussed in the Supporting Information (Figures S2 and S3). Here, we focus

DOI: 10.1021/acs.jpcc.9b08666
J. Phys. Chem. C 2019, 123, 24453−24460

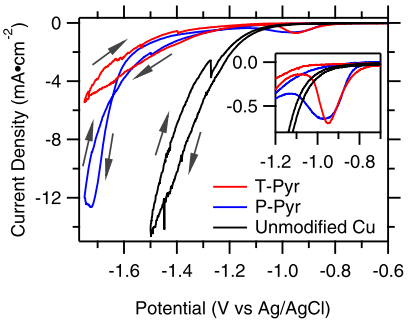

Figure 2. Cyclic voltammograms of Cu thin films in CO_2-saturated aqueous solutions of 0.5 M $KHCO_3$ in the absence (black) and presence of 10 mM P-Pyr (blue) and T-Pyr (red). The scan rate was 2 mV s^{-1}. The inset shows the waves because of the reductions of P-Pyr and T-Pyr.

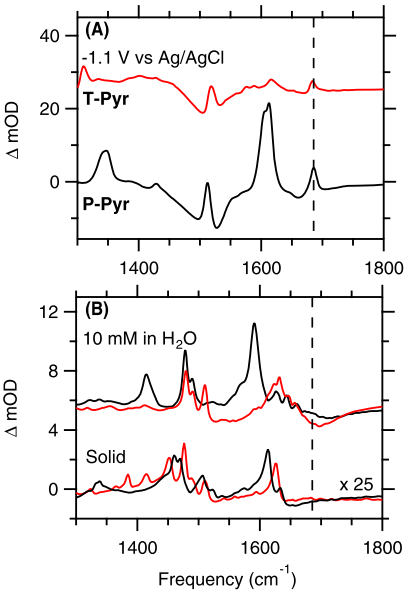

Figure 3. (A) IR spectra of the Cu/electrolyte interfaces in the presence of 10 mM T-Pyr (red) and 10 mM P-Pyr (black) in CO_2-saturated 0.5 M $KHCO_3$ at a potential of −1.1 V. The reference spectrum was taken at −0.6 V immediately before arylpyridiniums were added. The band indicated by the dashed line is consistent with the C═C stretch of an alkene. (B) Transmission IR spectra of solid-phase T-Pyr (red) and P-Pyr (black) and their aqueous solutions.

our discussion on the band at ≈1685 cm^{-1} (indicated by the dashed line in Figure 3A). A comparison of the interfacial spectra with those of solid and solution-phase T-Pyr and P-Pyr (Figure 3B) shows that the ≈1685 cm^{-1} band occurs only in the spectra of the interfaces. It is also absent in the spectrum of the Cu/electrolyte contact in the absence of T-Pyr and P-Pyr (Supporting Information, Figure S4). Taken together, these observations demonstrate that the ≈1685 cm^{-1} band arises from the film at the interface. The band's center frequency is consistent with the C═C stretch of an alkene group.[39] Dimerization of T-Pyr and P-Pyr leads to the destruction of the aromaticity of one of the ring systems, thereby resulting in the formation of alkene groups (Figure 1). Therefore, the observation of the band supports the notion that T-Pyr and P-Pyr dimerize during their reductive deposition on the Cu electrode.

The presence of the films significantly lowers the overall reduction currents compared to that observed for the unmodified Cu/electrolyte interface (Figure 2). The origin of the lower currents can be deduced from the partial currents for each product measured at a potential of −1.1 V versus a reversible hydrogen electrode (RHE) by Han and co-workers.[26] For the cyclic voltammograms with the organic films (Figure 2), the cathodic turning potential corresponds to −1.1 V versus an RHE. Our rough Cu thin films have an active surface area that is ≈10 times larger than that of a smooth polycrystalline Cu electrode. Therefore, our absolute currents are larger than those observed by Han and co-workers. However, the ratio of the currents at the turning potential is in good agreement with that reported by Han and co-workers. Therefore, on the basis of the results reported by Han et al. (Table 1), the lower current for T-Pyr-modified Cu/electrolyte interfaces primarily originates from the >10 times lower partial currents for methane and hydrogen compared to those of the unmodified Cu/electrolyte interface. By contrast, the comparatively lower current for the P-Pyr-modified Cu/electrolyte contact is mainly because of the negligibly small partial currents for hydrocarbons.

Following the reduction waves at −0.9 V, the broad-band survey IR spectra of the organic films show little variation during the cathodic forward and anodic backward scans (Supporting Information, Figures S2 and S3). This observation suggests that the reductions of T-Pyr and P-Pyr are self-limiting once the organic films have formed. Below, we will focus on the anodic backward scans of the cyclic voltammograms. However, the observations reported in the following also hold for the cathodic forward scans.

Effect of T-Pyr on Interfacial Characteristics. Figure 4 shows the IR spectra at the three different interfaces in the 1300−1600 cm^{-1} region. The spectra represent the change in the optical density of the interface that results when the electrode potential is increased from the indicated sample potential to the reference potential at −0.6 V at the end of the anodic scan of the cyclic voltammogram. The bands around 1330/1350 and 1515 cm^{-1} in the presence of T-Pyr (Figure 4A) and P-Pyr (Figure 4B) correspond to the Stark shifts of film-related vibrational modes. The broad negative band at ≈1525 cm^{-1} for the unmodified Cu/electrolyte interface (Figure 4C) arises from the desorption of the surface-bound carbonate and/or bicarbonate.[40,41]

At the T-Pyr-modified Cu/electrolyte interface, a prominent and a broad band appears at ≈1410 cm^{-1} at potentials close to the cathodic end of the cyclic voltammogram (Figure 4A). The band decreases as the potential is tuned more positively. Although a similar band is present at the P-Pyr-modified Cu/electrolyte interface (Figure 4B), its amplitude is substantially smaller. Similarly, at the unmodified Cu/electrolyte interface, the band is virtually absent (Figure 4C). Taken together, these observations show that the T-Pyr-modified Cu/electrolyte contact distinguishes itself from the other two interfaces by the comparatively larger amplitude of the band at ≈1410 cm^{-1}. Duplicate experiments demonstrate the reproducibility of the results (Supporting Information, Figures S2 and S3).

At the Cu/electrolyte interface, a band at this position has previously been assigned to the out-of-phase stretching vibrations of the solution-phase carbonate (CO_3^{2-}) in the vicinity of the electrode.[38,42−44] This assignment is reasonable for the following reasons:

1 Although several other interfacial species in the electrochemical CO_2 reduction are predicted to exhibit

DOI: 10.1021/acs.jpcc.9b08666
J. Phys. Chem. C 2019, 123, 24453−24460

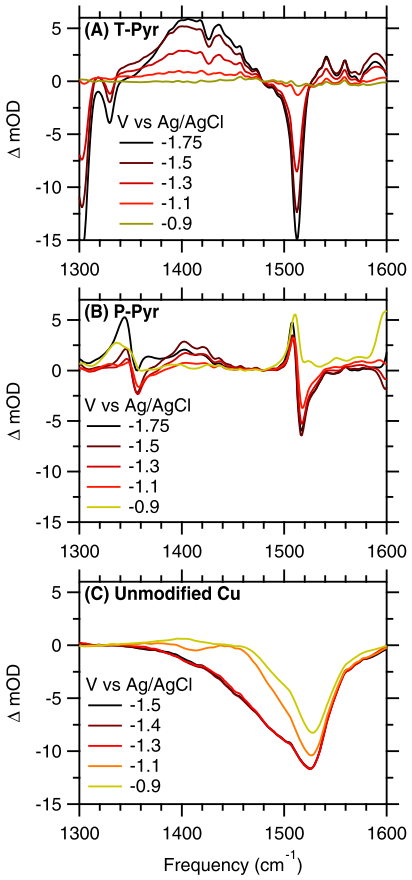

Figure 4. Potential-dependence of the carbonate band (≈1410 cm^{-1}) during the anodic reverse scan of the cyclic voltammogram (Figure 2) in (A) the presence of 10 mM T-Pyr, (B) in the presence of 10 mM P-Pyr, and (C) in the absence of additives. The final spectrum at the anodic end of the scan (−0.6 V) served as the reference spectrum.

bands in this region,[45] most species are intermediates whose surface concentrations are expected to be very low. Therefore, their detection is improbable.

2 The IR transmission spectrum of an aqueous solution of 10 mM K_2CO_3 shows a band at a similar position and with a comparable width (Supporting Information, Figure S5).

3 Every electron transfer in CO_2 reduction and hydrogen evolution produces a hydroxide ion according to

$$A + H_2O + e^- \rightarrow B + OH^- \quad (1)$$

where A and B represent oxidized and reduced species, respectively. Therefore, in the absence of an efficient mass transport at the electrode/electrolyte contact, the local pH in the vicinity of the electrode increases because of the Faradaic current. This increase in local pH leads to the deprotonation of the electrolyte's bicarbonate anions

$$HCO_3^- + OH^- \rightarrow CO_3^{2-} + H_2O \quad (2)$$

To test if the band's amplitude correlates with the mass transport conditions at the interface, we recorded the IR spectra of the unmodified Cu/electrolyte interface at a potential of −1.5 V with and without stirring the electrolyte. Figure 5A shows the appearance of the band after the stirring of the electrolyte was stopped at t = 0 s. Figure 5B demonstrates the disappearance of the band within a few seconds after stirring was resumed at t = 0 s. These findings

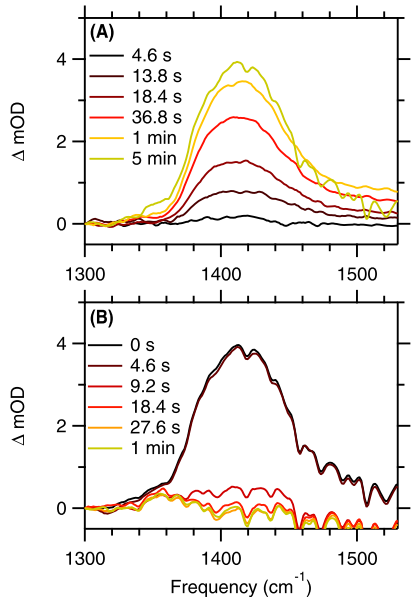

Figure 5. Time evolution of the carbonate band at the unmodified Cu/electrolyte interface with the Cu electrode held at a potential of −1.5 V: (A) after stirring of the electrolyte was stopped and (B) after stirring at 900 rpm was resumed. The stop/start time is t = 0 s in each panel. The reference spectrum was taken at −1.5 V, right before the stirring was initially stopped.

confirm that the appearance of the band is linked to the poor mass transport at the interface. On the basis of the position of the band and the large source of bicarbonate in the employed electrolyte, we attribute the band to the solution-phase CO_3^{2-} produced according to reaction 2. Therefore, an increase in the band indicates an increase in the local pH in the vicinity of the electrode.

Inspection of Figure 2 shows that the lowest electrochemical current is observed for the T-Pyr-modified Cu/electrolyte interface. On the basis of the current densities, one might expect the smallest increase in local pH to occur at that interface. Contrary to this expectation, the largest pH increase occurs at the T-Pyr-modified Cu/electrolyte interface, as evidenced by the comparatively large increase in the CO_3^{2-} band (Figure 4). Scanning electron microscopy (SEM) imaging of the T-Pyr- and P-Pyr-derived films shows that they exhibit distinct surface structures (Supporting Information, Figure S6). Taken together, the results indicate that the T-Pyr-derived film limits the interfacial mass transport because of its unique morphology, thereby leading to an accumulation of hydroxide in the vicinity of the electrode.

An increase in pH at the Cu/electrolyte contact has previously been demonstrated to lower the rates of hydrogen and methane evolution, whereas the rate of ethylene formation has been shown to be indifferent to pH changes.[10,11,48] An increase in local pH has also been invoked to explain the increases in CO_2 reduction selectivity on porous metal electrodes.[49−51] A high (local) pH limits the availability of surface-adsorbed hydrogen, the common reaction intermediate during the formation of methane and dihydrogen.[52] Our IR spectroscopic results unequivocally demonstrate a comparatively high pH gradient at the T-Pyr-modified Cu/electrolyte interface (Figure 4). As a result, the rates of hydrogen and methane formation are reduced in the presence of T-Pyr-derived films.

DOI: 10.1021/acs.jpcc.9b08666
J. Phys. Chem. C 2019, 123, 24453−24460

Effect of P-Pyr on the Adsorption of CO. Having elucidated the mechanism by which the T-Pyr-derived film alters the product selectivity, we now turn to the P-Pyr-modified Cu/electrolyte contact. In the presence of P-Pyr-derived films, little to no hydrocarbon evolution is observed, and hydrogen evolution is essentially not impacted with respect to the unmodified Cu/electrolyte contact (Table 1). To investigate the physical origin of this change in selectivity, we analyzed the C≡O stretch band of atop-bound CO (CO_{atop}) on the Cu electrode in the presence and absence of the films. CO_{atop} is an on-pathway intermediate in the electrochemical reduction of CO_2.[53,54]

Figure 6 shows the C≡O stretch bands of CO_{atop} at a potential of −1.5 V for the three different interfaces. The

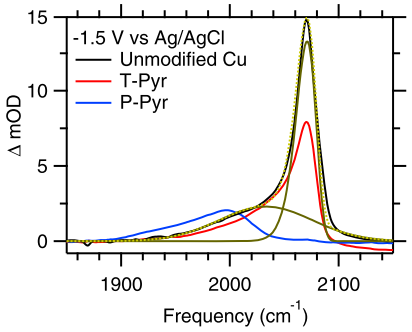

Figure 6. Comparison of the C≡O stretch bands of CO_{atop} on Cu at an applied potential of −1.5 V at the three different interfaces as indicated. The green dashed line represents a fit of the model, the sum of the two (skewed) Gaussian functions,[46,47] to the spectrum of CO_{atop} at the unmodified Cu electrode (black). The solid green lines represent the Gaussian functions.

lineshape for CO_{atop} on the unmodified Cu electrode is markedly asymmetric. The lineshape is well described by the sum of a broad and a narrow Gaussian function (green lines): the narrow band at ≈2070 cm^{-1} is due to CO_{atop} on the undercoordinated Cu sites (step and kink sites), whereas the broad band at ≈2040 cm^{-1} arises from CO_{atop} on comparatively more highly coordinated Cu sites (terrace sites).[47] In the following, we will refer to the narrow band at ≈2070 cm^{-1} as the high-frequency band (HFB). The integrated band areas of the two bands do not directly reflect the relative population of CO_{atop} on the two different types of sites: the large amplitude of the ≈2070 cm^{-1} band (relative to the broad band) may be a manifestation of intensity borrowing because of dynamical dipole coupling.[55−57]

The C≡O stretch frequency and lineshape of CO_{atop} for the T-Pyr-modified interface are comparable to that for the unmodified Cu/electrolyte contact. This observation demonstrates that the T-Pyr-derived film does not significantly alter the interaction of CO with the Cu surface. By stark contrast, the HFB is absent in the presence of P-Pyr. This observation suggests that P-Pyr partially blocks CO adsorption sites. In contrast to T-Pyr, P-Pyr contains a nitrogen atom with an electron lone pair (Figure 1). We hypothesized that the presence of the lone pair enables P-Pyr to compete with CO for adsorption sites.

The disappearance of the HFB in the presence of P-Pyr could be caused by at least two distinct mechanisms:

1 P-Pyr may indiscriminately bind to a variety of Cu sites, thereby producing a low CO_{atop} coverage. Dynamical dipole coupling is weak under low-coverage conditions. The absence of significant intensity borrowing under these conditions may prevent the observation of the HFB.
2 P-Pyr may preferentially bind to undercoordinated Cu sites, thereby blocking CO from adsorbing on these sites.

To test the first hypothesis, we monitored the C≡O stretch frequency at the unmodified Cu/electrolyte contact at a fixed potential as a function of coverage. To this end, we saturated the electrolyte with CO_2 to produce CO_{atop}. We then switched the purge gas to Ar to continuously lower the CO_{atop} coverage. The C≡O stretch band with a peak amplitude of ≈1/5 compared to that observed at saturation coverage is representative of the spectrum at a low CO_{atop} coverage on an unmodified Cu electrode. Even at this low coverage, we observe the HFB (Supporting Information, Figure S7). Therefore, a low CO_{atop} coverage cannot solely account for the absence of the HFB.

To test the second hypothesis, we conducted studies on CO-saturated electrolyte containing pyridine. Pyridine also possesses a nitrogen atom with a lone pair, but it does not form a visible deposit on the electrode under reduction conditions. Like P-Pyr, pyridine also suppresses hydrocarbon formation.[26] To test if pyridine competes with CO for surface sites, we first saturated the electrode surface with CO by purging the electrolyte with CO gas and by applying a potential of −1.3 V. Then, we added pyridine to the electrolyte in a stepwise manner and monitored the change in the C≡O stretch lineshape of CO_{atop}. As shown in Figure 7, with an

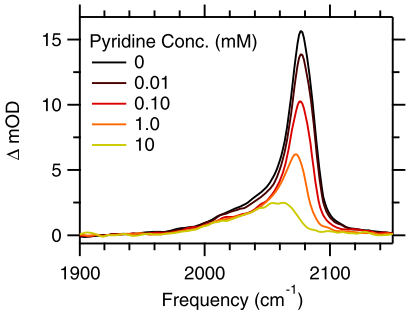

Figure 7. Evolution of the C≡O stretch bands as the concentration of pyridine in the electrolyte increases and the potential is maintained at −1.3 V in the CO-saturated electrolyte.

increasing concentration of pyridine in the electrolyte, the HFB decreases and eventually completely disappears. The resulting C≡O stretch spectrum is similar to that observed in the presence of P-Pyr, suggesting that both additives similarly impact CO adsorption. Taken together, these observations suggest that pyridine and P-Pyr selectively poison undercoordinated Cu sites.

It is important to note that a significant population of CO_{atop} remains on the electrode in the presence of P-Pyr (Figure 6). However, no significant formation of hydrocarbons occurs at the P-Pyr-modifed interface (Table 1). These observations implicate undercoordinated Cu sites as the catalytically actives sites in the reduction of CO to hydrocarbons. This conclusion is consistent with prior reports.[58−60]

Because of the weak vibrational bands associated with the surface-adsorbed pyridine, its coverage is difficult to quantify.

DOI: 10.1021/acs.jpcc.9b08666
J. Phys. Chem. C 2019, 123, 24453−24460

Prior studies have shown that pyridine adsorbs on Cu and other metal electrodes in an end-on configuration with the nitrogen bound to a surface metal atom.[61−63] As shown in the Supporting Information (Figure S8), our spectroscopic data are consistent with these prior findings. These observations support the notion that the electron lone pair of the nitrogen atom enables pyridine and P-Pyr to compete with CO for adsorption sites.

CONCLUSIONS

In summary, we investigated the effects of two *N*-substituted arylpyridinium ions (T-Pyr and P-Pyr) on the properties of the Cu/electrolyte interface during CO_2 reduction. Using SEIRAS, we showed that the interfacial pH in the vicinity of the T-Pyr-modified Cu electrode increases at moderate current densities (<5 mA cm^{-2}). By contrast, such an increase in interfacial pH does not occur on unmodified Cu electrodes or those with P-Pyr-derived films, even though protons are consumed at these interfaces at relatively faster rates. This observation suggests that T-Pyr-derived films impede the mass transport to/from the Cu surface. The resulting lower availability of protons provides a rationale for the reported suppression of H_2 and CH_4 formation and minimal impact on $C_{\geq 2}$ hydrocarbon production rates in the presence of this film. Further, we showed that the adsorption of CO_{atop} is significantly impacted by P-Pyr-derived films. Specifically, our results suggest that P-Pyr selectively poisons undercoordinated Cu adsorption sites, thereby blocking CO from adsorbing on these sites. As a result, further hydrogenation of CO to hydrocarbons is impeded in the presence of this compound. Our results indicate that N-heterocycles that contain an electron lone pair on the nitrogen atom are detrimental to CO_2 reduction because the presence of the lone pair facilitates binding of these compounds to the active sites. Further, our study implicates undercoordinated Cu sites as the active sites in the electrocatalytic reduction of CO to hydrocarbons.

EXPERIMENTAL PROCEDURES

1-(4-Pyridyl)pyridinium chloride hydrochloride (TCI Chemicals, >98%) and pyridine (Fisher Chemical, >99%) were used as received. 1-(4-Tolyl)pyridinium chloride was synthesized from 1-(2,4-dinitrophenyl)pyridinium chloride (Oakwood Chemicals, 97%) and *p*-toluidine (Sigma-Aldrich, 99%) according to the reported methods and purified with silica flash chromatography.[64] $KHCO_3$ (≥99.98%) was obtained from Sigma-Aldrich. High purity water (18.2 MΩ cm) was sourced from a Barnstead Nanopure Diamond system and used for all experiments. CO_2 (research grade) and Ar (ultra high purity) were procured from Air Gas.

SEIRAS measurements were carried out in a custom two-compartment polyetheretherketone/glass cell (Supporting Information, Figure S1) with stirring capabilities and placed into a horizontally mounted ATR accessory (VeeMax III; Pike Technologies; Madison, WI).[38] A Ag/AgCl reference electrode (3 M NaCl; Basi Inc.; West Lafayette, IN) and a graphite rod (99.995%; 3 mm thick; Sigma-Aldrich) were used as the reference and counter electrodes, respectively. The potential was controlled with a Versastat 3 potentiostat (AMETEK; Berwyn, PA). The Ohmic resistance was measured using VersaSTAT 3 with the Versastudio software. An 85% of the Ohmic resistance was compensated during measurements. Copper thin-film preparation and the employed spectroscopic and electrochemical methods were described previously.[37,41,65]

ASSOCIATED CONTENT

Supporting Information

The Supporting Information is available free of charge on the ACS Publications website at DOI: 10.1021/acs.jpcc.9b08666.

Schematic of the electrochemical cell/SEIRAS setup; potential-dependent IR spectra of T-Pyr- and P-Pyr-modified Cu/electrolyte interfaces; IR spectrum of the unmodified Cu/electrolyte interface; IR spectrum of solution carbonate; SEM images of Cu surfaces with T-Pyr- and P-Pyr-derived films; coverage-dependent IR spectra of CO_{atop}; IR spectra of solution-phase and surface-adsorbed pyridine; NMR spectrum of the synthesized T-Pyr; and gas chromatography−mass spectrometry product analysis during electrolysis in the presence of T-Pyr (PDF)

AUTHOR INFORMATION

Corresponding Author

*E-mail: waegele@bc.edu.

ORCID

Vincent J. Ovalle: 0000-0002-0586-222X

Matthias M. Waegele: 0000-0002-1186-7545

Notes

The authors declare no competing financial interest.

ACKNOWLEDGMENTS

This work was supported by a CAREER award from the National Science Foundation (award no. CHE-1847841).

REFERENCES

(1) Hori, Y.; Kikuchi, K.; Suzuki, S. Production of CO and CH_4 in Electrochemical Reduction of CO_2 at Metal Electrodes in Aqueous Hydrogencarbonate Solution. *Chem. Lett.* **1985**, 1695−1698.

(2) Kuhl, K. P.; Hatsukade, T.; Cave, E. R.; Abram, D. N.; Kibsgaard, J.; Jaramillo, T. F. Electrocatalytic Conversion of Carbon Dioxide to Methane and Methanol on Transition Metal Surfaces. *J. Am. Chem. Soc.* **2014**, *136*, 14107−14113.

(3) Hori, Y.; Murata, A.; Takahashi, R. Formation of Hydrocarbons in the Electrochemical Reduction of Carbon Dioxide at a Copper Electrode in Aqueous Solution. *J. Chem. Soc., Faraday Trans. 1* **1989**, *85*, 2309−2326.

(4) Kuhl, K. P.; Cave, E. R.; Abram, D. N.; Jaramillo, T. F. New Insights into the Electrochemical Reduction of Carbon Dioxide on Metallic Copper Surfaces. *Energy Environ. Sci.* **2012**, *5*, 7050−7059.

(5) Luo, W.; Nie, X.; Janik, M. J.; Asthagiri, A. Facet Dependence of CO_2 Reduction Paths on Cu Electrodes. *ACS Catal.* **2016**, *6*, 219−229.

(6) Huang, Y.; Handoko, A. D.; Hirunsit, P.; Yeo, B. S. Electrochemical Reduction of CO_2 Using Copper Single-Crystal Surfaces: Effects of CO* Coverage on the Selective Formation of Ethylene. *ACS Catal.* **2017**, *7*, 1749−1756.

(7) Verma, S.; Kim, B.; Jhong, H.-R. M.; Ma, S.; Kenis, P. J. A. A Gross-Margin Model for Defining Technoeconomic Benchmarks in the Electroreduction of CO_2. *ChemSusChem* **2016**, *9*, 1972−1979.

(8) Jouny, M.; Luc, W.; Jiao, F. General Techno-Economic Analysis of CO_2 Electrolysis Systems. *Ind. Eng. Chem. Res.* **2018**, *57*, 2165−2177.

(9) De Luna, P.; Hahn, C.; Higgins, D.; Jaffer, S. A.; Jaramillo, T. F.; Sargent, E. H. What Would It Take for Renewably Powered Electrosynthesis to Displace Petrochemical Processes? *Science* **2019**, *364*, No. eaav3506.

(10) Kas, R.; Kortlever, R.; Yılmaz, H.; Koper, M. T. M.; Mul, G. Manipulating the Hydrocarbon Selectivity of Copper Nanoparticles in CO_2 Electroreduction by Process Conditions. *ChemElectroChem* **2015**, *2*, 354−358.
(11) Varela, A. S.; Kroschel, M.; Reier, T.; Strasser, P. Controlling the Selectivity of CO_2 Electroreduction on Copper: The Effect of the Electrolyte Concentration and the Importance of the Local pH. *Catal. Today* **2016**, *260*, 8−13.
(12) Hori, Y.; Takahashi, I.; Koga, O.; Hoshi, N. Selective Formation of C2 Compounds from Electrochemical Reduction of CO_2 at a Series of Copper Single Crystal Electrodes. *J. Phys. Chem. B* **2002**, *106*, 15−17.
(13) Schouten, K. J. P.; Pérez Gallent, E.; Koper, M. T. M. Structure Sensitivity of the Electrochemical Reduction of Carbon Monoxide on Copper Single Crystals. *ACS Catal.* **2013**, *3*, 1292−1295.
(14) Li, C. W.; Ciston, J.; Kanan, M. W. Electroreduction of Carbon Monoxide to Liquid Fuel on Oxide-Derived Nanocrystalline Copper. *Nature* **2014**, *508*, 504−507.
(15) Loiudice, A.; Lobaccaro, P.; Kamali, E. A.; Thao, T.; Huang, B. H.; Ager, J. W.; Buonsanti, R. Tailoring Copper Nanocrystals Towards C_2 Products in Electrochemical CO_2 Reduction. *Angew. Chem., Int. Ed.* **2016**, *55*, 5789−5792.
(16) Hahn, C.; Hatsukade, T.; Kim, Y.-G.; Vailionis, A.; Baricuatro, J. H.; Higgins, D. C.; Nitopi, S. A.; Soriaga, M. P.; Jaramillo, T. F. Engineering Cu Surfaces for the Electrocatalytic Conversion of CO_2: Controlling Selectivity Toward Oxygenates and Hydrocarbons. *Proc. Natl. Acad. Sci. U.S.A.* **2017**, *114*, 5918−5923.
(17) Weng, Z.; Wu, Y.; Wang, M.; Jiang, J.; Yang, K.; Huo, S.; Wang, X.-F.; Ma, Q.; Brudvig, G. W.; Batista, V. S.; et al. Active Sites of Copper-complex Catalytic Materials for Electrochemical Carbon Dioxide Reduction. *Nat. Commun.* **2018**, *9*, 415.
(18) Ma, S.; Sadakiyo, M.; Luo, R.; Heima, M.; Yamauchi, M.; Kenis, P. J. A. One-Step Electrosynthesis of Ethylene and Ethanol from CO_2 in an Alkaline Electrolyzer. *J. Power Sources* **2016**, *301*, 219−228.
(19) Reller, C.; Krause, R.; Volkova, E.; Schmid, B.; Neubauer, S.; Rucki, A.; Schuster, M.; Schmid, G. Selective Electroreduction of CO_2 Toward Ethylene on Nano Dendritic Copper Catalysts at High Current Density. *Adv. Energy Mater.* **2017**, *7*, 1602114.
(20) Dinh, C.-T.; Burdyny, T.; Kibria, M. G.; Seifitokaldani, A.; Gabardo, C. M.; García de Arquer, F. P.; Kiani, A.; Edwards, J. P.; De Luna, P.; Bushuyev, O. S.; et al. CO_2 Electroreduction to Ethylene via Hydroxide-mediated Copper Catalysis at an Abrupt Interface. *Science* **2018**, *360*, 783−787.
(21) Jouny, M.; Luc, W.; Jiao, F. High-Rate Electroreduction of Carbon Monoxide to Multi-carbon Products. *Nat. Catal.* **2018**, *1*, 748−755.
(22) Barton, E. E.; Rampulla, D. M.; Bocarsly, A. B. Selective Solar-Driven Reduction of CO_2 to Methanol Using a Catalyzed p-GaP Based Photoelectrochemical Cell. *J. Am. Chem. Soc.* **2008**, *130*, 6342−6344.
(23) Tornow, C. E.; Thorson, M. R.; Ma, S.; Gewirth, A. A.; Kenis, P. J. A. Nitrogen-Based Catalysts for the Electrochemical Reduction of CO_2 to CO. *J. Am. Chem. Soc.* **2012**, *134*, 19520−19523.
(24) Xie, M. S.; Xia, B. Y.; Li, Y.; Yan, Y.; Yang, Y.; Sun, Q.; Chan, S. H.; Fisher, A.; Wang, X. Amino Acid Modified Copper Electrodes for the Enhanced Selective Electroreduction of Carbon Dioxide Towards Hydrocarbons. *Energy Environ. Sci.* **2016**, *9*, 1687−1695.
(25) Fang, Y.; Flake, J. C. Electrochemical Reduction of CO_2 at Functionalized Au Electrodes. *J. Am. Chem. Soc.* **2017**, *139*, 3399−3405.
(26) Han, Z.; Kortlever, R.; Chen, H.-Y.; Peters, J. C.; Agapie, T. CO_2 Reduction Selective for $C_{\geq 2}$ Products on Polycrystalline Copper with N-Substituted Pyridinium Additives. *ACS Cent. Sci.* **2017**, *3*, 853−859.
(27) Gong, M.; Cao, Z.; Liu, W.; Nichols, E. M.; Smith, P. T.; Derrick, J. S.; Liu, Y.-S.; Liu, J.; Wen, X.; Chang, C. J. Supramolecular Porphyrin Cages Assembled at Molecular-Materials Interfaces for Electrocatalytic CO Reduction. *ACS Cent. Sci.* **2017**, *3*, 1032−1040.
(28) Hoang, T. T. H.; Ma, S.; Gold, J. I.; Kenis, P. J. A.; Gewirth, A. A. Nanoporous Copper Films by Additive-Controlled Electrodeposition: CO_2 Reduction Catalysis. *ACS Catal.* **2017**, *7*, 3313−3321.
(29) Ahn, S.; Klyukin, K.; Wakeham, R. J.; Rudd, J. A.; Lewis, A. R.; Alexander, S.; Carla, F.; Alexandrov, V.; Andreoli, E. Poly-Amide Modified Copper Foam Electrodes for Enhanced Electrochemical Reduction of Carbon Dioxide. *ACS Catal.* **2018**, *8*, 4132−4142.
(30) Kauffman, D. R.; Alfonso, D. R.; Tafen, D. N.; Wang, C.; Zhou, Y.; Yu, Y.; Lekse, J. W.; Deng, X.; Espinoza, V.; Trindell, J.; et al. Selective Electrocatalytic Reduction of CO_2 into CO at Small, Thiol-Capped Au/Cu Nanoparticles. *J. Phys. Chem. C* **2018**, *122*, 27991−28000.
(31) Wang, Z.; Wu, L.; Sun, K.; Chen, T.; Jiang, Z.; Cheng, T.; Goddard, W. A. Surface Ligand Promotion of Carbon Dioxide Reduction through Stabilizing Chemisorbed Reactive Intermediates. *J. Phys. Chem. Lett.* **2018**, *9*, 3057−3061.
(32) Iijima, G.; Kitagawa, T.; Katayama, A.; Inomata, T.; Yamaguchi, H.; Suzuki, K.; Hirata, K.; Hijikata, Y.; Ito, M.; Masuda, H. CO_2 Reduction Promoted by Imidazole Supported on a Phosphonium-Type Ionic-Liquid-Modified Au Electrode at a Low Overpotential. *ACS Catal.* **2018**, *8*, 1990−2000.
(33) Buckley, A. K.; Lee, M.; Cheng, T.; Kazantsev, R. V.; Larson, D. M.; Goddard, W. A., III; Toste, F. D.; Toma, F. M. Electrocatalysis at Organic−Metal Interfaces: Identification of Structure−Reactivity Relationships for CO_2 Reduction at Modified Cu Surfaces. *J. Am. Chem. Soc.* **2019**, *141*, 7355−7364.
(34) Banerjee, S.; Han, X.; Thoi, V. S. Modulating the Electrode-Electrolyte Interface with Cationic Surfactants in Carbon Dioxide Reduction. *ACS Catal.* **2019**, *9*, 5631−5637.
(35) Wang, J.; Zhang, F.; Kang, X.; Chen, S. Organic Functionalization of Metal Catalysts: Enhanced Activity Towards Electroreduction of Carbon Dioxide. *Curr. Opin. Electrochem.* **2019**, *13*, 40−46.
(36) Schmitt, K. G.; Gewirth, A. A. In Situ Surface-Enhanced Raman Spectroscopy of the Electrochemical Reduction of Carbon Dioxide on Silver with 3,5-Diamino-1,2,4-Triazole. *J. Phys. Chem. C* **2014**, *118*, 17567−17576.
(37) Gunathunge, C. M.; Ovalle, V. J.; Li, Y.; Janik, M. J.; Waegele, M. M. Existence of an Electrochemically Inert CO Population on Cu Electrodes in Alkaline pH. *ACS Catal.* **2018**, *8*, 7507−7516.
(38) Dunwell, M.; Yang, X.; Setzler, B. P.; Anibal, J.; Yan, Y.; Xu, B. Examination of Near-Electrode Concentration Gradients and Kinetic Impacts on the Electrochemical Reduction of CO_2 using Surface-Enhanced Infrared Spectroscopy. *ACS Catal.* **2018**, *8*, 3999−4008.
(39) Larkin, P. J. *Infrared and Raman Spectroscopy; Principles and Spectral Interpretation*; Elsevier, 2011.
(40) Hori, Y.; Koga, O.; Watanabe, Y.; Matsuo, T. FTIR Measurements of Charge Displacement Adsorption of CO on Poly- and Single Crystal (100) of Cu Electrodes. *Electrochim. Acta* **1998**, *44*, 1389−1395.
(41) Gunathunge, C. M.; Ovalle, V. J.; Waegele, M. M. Probing Promoting Effects of Alkali Cations on the Reduction of CO at the Aqueous Electrolyte/Copper Interface. *Phys. Chem. Chem. Phys.* **2017**, *19*, 30166−30172.
(42) Rudolph, W. W.; Fischer, D.; Irmer, G. Vibrational Spectroscopic Studies and Density Functional Theory Calculations of Speciation in the CO_2-Water System. *Appl. Spectrosc.* **2006**, *60*, 130−144.
(43) Baldassarre, M.; Barth, A. The Carbonate/Bicarbonate System as a pH Indicator for Infrared Spectroscopy. *Analyst* **2014**, *139*, 2167−2176.
(44) Zhu, S.; Jiang, B.; Cai, W.-B.; Shao, M. Direct Observation on Reaction Intermediates and the Role of Bicarbonate Anions in CO_2 Electrochemical Reduction Reaction on Cu Surfaces. *J. Am. Chem. Soc.* **2017**, *139*, 15664−15667.
(45) Cheng, T.; Fortunelli, A.; Goddard, W. A., III Reaction Intermediates During Operando Electrocatalysis Identified from Full

DOI: 10.1021/acs.jpcc.9b08666
J. Phys. Chem. C 2019, 123, 24453−24460

Solvent Quantum Mechanics Molecular Dynamics. *Proc. Natl. Acad. Sci. U.S.A.* **2019**, *116*, 7718−7722.
(46) Stancik, A. L.; Brauns, E. B. A Simple Asymmetric Lineshape for Fitting Infrared Absorption Spectra. *Vib. Spectrosc.* **2008**, *47*, 66−69.
(47) Gunathunge, C. M.; Li, X.; Li, J.; Hicks, R. P.; Ovalle, V. J.; Waegele, M. M. Spectroscopic Observation of Reversible Surface Reconstruction of Copper Electrodes under CO_2 Reduction. *J. Phys. Chem. C* **2017**, *121*, 12337−12344.
(48) Schouten, K. J. P.; Pérez Gallent, E.; Koper, M. T. The Influence of pH on the Reduction of CO and CO_2 to Hydrocarbons on Copper Electrodes. *J. Electroanal. Chem.* **2014**, *716*, 53−57.
(49) Hall, A. S.; Yoon, Y.; Wuttig, A.; Surendranath, Y. Mesostructure-Induced Selectivity in CO_2 Reduction Catalysis. *J. Am. Chem. Soc.* **2015**, *137*, 14834−14837.
(50) Ma, M.; Djanashvili, K.; Smith, W. A. Controllable Hydrocarbon Formation from the Electrochemical Reduction of CO_2 Over Cu Nanowire Arrays. *Angew. Chem., Int. Ed.* **2016**, *55*, 6680−6684.
(51) Yoon, Y.; Hall, A. S.; Surendranath, Y. Tuning of Silver Catalyst Mesostructure Promotes Selective Carbon Dioxide Conversion into Fuels. *Angew. Chem., Int. Ed.* **2016**, *55*, 15282−15286.
(52) Schreier, M.; Yoon, Y.; Jackson, M. N.; Surendranath, Y. Competition between H and CO for Active Sites Governs Copper-Mediated Electrosynthesis of Hydrocarbon Fuels. *Angew. Chem., Int. Ed.* **2018**, *57*, 10221−10225.
(53) Hori, Y.; Murata, A.; Yoshinami, Y. Adsorption of CO, Intermediately Formed in Electrochemical Reduction of CO_2, at a Copper Electrode. *J. Chem. Soc., Faraday Trans.* **1991**, *87*, 125−128.
(54) Peterson, A. A.; Abild-Pedersen, F.; Studt, F.; Rossmeisl, J.; Nørskov, J. K. How Copper Catalyzes the Electroreduction of Carbon Dioxide into Hydrocarbon Fuels. *Energy Environ. Sci.* **2010**, *3*, 1311−1315.
(55) Hollins, P.; Davies, K. J.; Pritchard, J. Infrared Spectra of CO Chemisorbed on a Surface Vicinal to Cu(110): The Influence of Defect Sites. *Surf. Sci.* **1984**, *138*, 75−83.
(56) Borguet, E.; Dai, H.-L. Site-specific Properties and Dynamical Dipole Coupling of CO Molecules Adsorbed on a Vicinal Cu(100) Surface. *J. Chem. Phys.* **1994**, *101*, 9080−9095.
(57) Borguet, E.; Dai, H.-L. Probing Surface Short Range Order and Inter-Adsorbate Interactions through IR Vibrational Spectroscopy: CO on Cu(100). *J. Phys. Chem. B* **2005**, *109*, 8509−8512.
(58) Tang, W.; Peterson, A. A.; Varela, A. S.; Jovanov, Z. P.; Bech, L.; Durand, W. J.; Dahl, S.; Nørskov, J. K.; Chorkendorff, I. The Importance of Surface Morphology in Controlling the Selectivity of Polycrystalline Copper for CO_2 Electroreduction. *Phys. Chem. Chem. Phys.* **2012**, *14*, 76−81.
(59) Verdaguer-Casadevall, A.; Li, C. W.; Johansson, T. P.; Scott, S. B.; McKeown, J. T.; Kumar, M.; Stephens, I. E. L.; Kanan, M. W.; Chorkendorff, I. Probing the Active Surface Sites for CO Reduction on Oxide-Derived Copper Electrocatalysts. *J. Am. Chem. Soc.* **2015**, *137*, 9808−9811.
(60) Cheng, T.; Xiao, H.; Goddard, W. A. Nature of the Active Sites for CO Reduction on Copper Nanoparticles; Suggestions for Optimizing Performance. *J. Am. Chem. Soc.* **2017**, *139*, 11642−11645.
(61) Haq, S.; King, D. A. Configurational Transitions of Benzene and Pyridine Adsorbed on Pt(111) and Cu(110) Surfaces: An Infrared Study. *J. Phys. Chem.* **1996**, *100*, 16957−16965.
(62) Wang, H.-F.; Yan, Y.-G.; Huo, S.-J.; Cai, W.-B.; Xu, Q.-J.; Osawa, M. Seeded Growth Fabrication of Cu-on-Si Electrodes for In Situ ATR-SEIRAS Applications. *Electrochim. Acta* **2007**, *52*, 5950−5957.
(63) Bruckbauer, A.; Otto, A. Raman Spectroscopy of Pyridine Adsorbed on Single Crystal Copper Electrodes. *J. Raman Spectrosc.* **1998**, *29*, 665−672.
(64) Zeghbib, N.; Thelliere, P.; Rivard, M.; Martens, T. Microwaves and Aqueous Solvents Promote the Reaction of Poorly Nucleophilic Anilines with a Zincke Salt. *J. Org. Chem.* **2016**, *81*, 3256−3262.
(65) Li, J.; Li, X.; Gunathunge, C. M.; Waegele, M. M. Hydrogen Bonding Steers the Product Selectivity of Electrocatalytic CO Reduction. *Proc. Natl. Acad. Sci. U.S.A.* **2019**, *116*, 9220−9229.

DOI: 10.1021/acs.jpcc.9b08666
J. Phys. Chem. C 2019, 123, 24453−24460